npj | climate and atmospheric science

Article

Published in partnership with CECCR at King Abdulaziz University

https://doi.org/10.1038/s41612-025-00983-4

Weakened influence of ENSO on the East Asian summer monsoon since the early 2000s

Check for updates

Tiantian Yu[1], Wen Chen[2,3] ✉, Ping Huang[1,4] ✉, Gang Huang[4,5] & Xianke Yang[6]

El Niño–Southern Oscillation (ENSO) was identified as the dominant factor influencing the East Asian summer monsoon (EASM), especially after the mid-1970s when the tropical Indian Ocean (TIO) response remarkably strengthened. Here, we find that the influence of ENSO on the EASM has been diminishing since the early 2000s. The EASM in wind anomalies associated with the positive phase of ENSO quickly disintegrates in August, changing from an anticyclone over the western North Pacific (WNPAC) to a cyclone over the western North Pacific (WNP), which exerts significant influence on the East Asia rainfall. These weakened EASM responses are closely linked to the changes in ENSO's rate of decay around the early 2000s. During 1977–1999, ENSO events peaking in the boreal winter frequently display a gradual decay, triggering robust positive ocean–atmosphere feedback, which extends beyond the TIO and involves the WNP. The resultant North Indian Ocean (NIO) warming develops and persists through the decaying summer, maintaining the WNPAC in August. In contrast, ENSO events exhibit a faster decay during 2000–2022, leading to a weakened ENSO-induced TIO feedback. Additionally, the WNP warms up, accompanied by the collapse of the easterly wind response, contributing to the weak summer peak in the NIO. In turn, the weak NIO warming rapidly decays, which cannot sustain the WNPAC in August. This study emphasizes the crucial role of WNP air–sea coupling in the changing influences of ENSO on the EASM.

The East Asian summer monsoon (EASM) is an essential system that affects the summer climate in highly populated East Asia. The western North Pacific anomalous anticyclone (WNPAC) is the dominant feature of the interannual variability of the EASM low-level circulation[1–5], which can induce droughts and floods causing serious casualties and economic losses[6,7]. The predictability of the EASM can be modulated by many factors[8–11], of which El Niño–Southern Oscillation (ENSO) has been identified as the most essential one, especially since the mid-1970s[3,12–16]. As the strongest air–sea coupled mode, ENSO can govern the EASM variability through modulating the low-level circulation over the western North Pacific (WNP)[1,3,14,17–22].

During the El Niño decaying phase, the warm sea surface temperature (SST) anomalies are weak and even dissipated in the central-eastern tropical Pacific, but their climatic impact lingers over the Indo-northwest Pacific region, maintaining the WNPAC via inter-basin ocean–atmosphere feedback[3,14,22–28]. Over the WNP, the anomalous northeasterlies on the southeast flank of the El Niño-induced WNPAC strengthen the northeast trade winds and contribute to the SST cooling over the WNP through the wind–evaporation–SST (WES) feedback[3]. In turn, this WNP SST cooling helps maintain the WNPAC via the atmospheric Rossby wave response[27,29]. For the tropical Indian Ocean (TIO), El Niño affects the southwest Indian Ocean mainly through westward-propagating oceanic Rossby waves, which induce the southwest Indian Ocean to warm up. This SST warming can further enhance the North Indian Ocean (NIO) warming by yielding equatorially antisymmetric wind anomalies[30,31]. The northeasterly wind anomalies to the north of the equator contribute to the NIO SST warming via positive WES feedback after the onset of the southwest monsoon[31]. Additionally, the anomalous easterlies on the south flank of the WNPAC

[1]Center for Monsoon System Research, Institute of Atmospheric Physics, Chinese Academy of Sciences, Beijing, China. [2]Yunnan Key Laboratory of Meteorological Disasters and Climate Resources in the Greater Mekong Subregion, Yunnan University, Kunming, China. [3]Yunnan International Joint Laboratory of Monsoon and Climate Disasters, Yunnan University, Kunming, China. [4]National Key Laboratory of Earth System Numerical Modeling and Application, Institute of Atmospheric Physics, Chinese Academy of Sciences, Beijing, China. [5]University of Chinese Academy of Sciences, Beijing, China. [6]MOA Key Laboratory of Crop Ecophysiology and Farming System in the Middle Reaches of the Yangtze River, College of Plant Science and Technology, Huazhong Agricultural University, Wuhan, China. ✉e-mail: chenwen-dq@ynu.edu.cn; huangping@mail.iap.ac.cn

can extend to the TIO, which also favors the NIO SST warming[26,27]. During the El Niño decaying summer, the resultant NIO warming forces warm Kelvin waves propagating equatorially towards the western Pacific and sustain the WNPAC by lower-level Ekman divergence[21,22,32]. All these ENSO-induced anomalies of NIO SST, WNP SST, and WNP low-level circulation feed back to each other and constitute an inter-basin coupled mode known as the Indo-western Pacific Ocean capacitor (IPOC)[14,26]. The IPOC mode directly influences the summertime WNPAC, which acts like a capacitor linking ENSO with the following EASM[14,24,25].

The inter-basin air–sea coupling of the IPOC has strongly influenced the EASM since the mid-1970s, which is largely modulated by the interdecadal change of ENSO[33–38]. However, ENSO experienced an another interdecadal shift around the beginning of the 2000s that featured an increase of frequency and a decrease of variability[39–42]. Associated with this climate regime shift, interdecadal variations in the East Asian climate systems have also been identified by recent studies[43–56]. The IPOC mode might have varied over the past few decades, forcing the response of the summer climate to the interdecadal change in ENSO. Yet, how the interdecadal change in ENSO influenced the EASM through the inter-basin coupling around the early 2000s remains to be elucidated. In this study, we found a weakened influence of ENSO on the EASM since the early 2000s, especially in the decaying August. This weakened EASM response is closely linked to the changes in ENSO's rate of decay and the resultant changing ocean–atmosphere feedback. Here, we highlight that the WNP air–sea coupling played a crucial role in changing the NIO feedback around the early 2000s. The findings shed light on ENSO's effect on the EASM and deepen our understanding of the IPOC mode, which is of great societal importance and economic value in terms of accurately predicting the EASM.

Results

Weakened impacts of ENSO on the EASM in August since the early 2000s

The impacts of ENSO on the EASM exhibit substantial interdecadal variations over the past few decades (Fig. 1). Based on the correlations between ENSO, NIO SST, and the EASM from 1958 to 2022 (Fig. 1a, b), we divided the research period (i.e., 1958–2022) into three sub-periods (1958–1974, 1977–1999, 2000–2022). The EASM responses enhanced from 1975 (Fig. 1a–d), as reported previously[36,38], but experienced a new interdecadal transition around the early 2000s (Fig. 1a, b). This weakened EASM

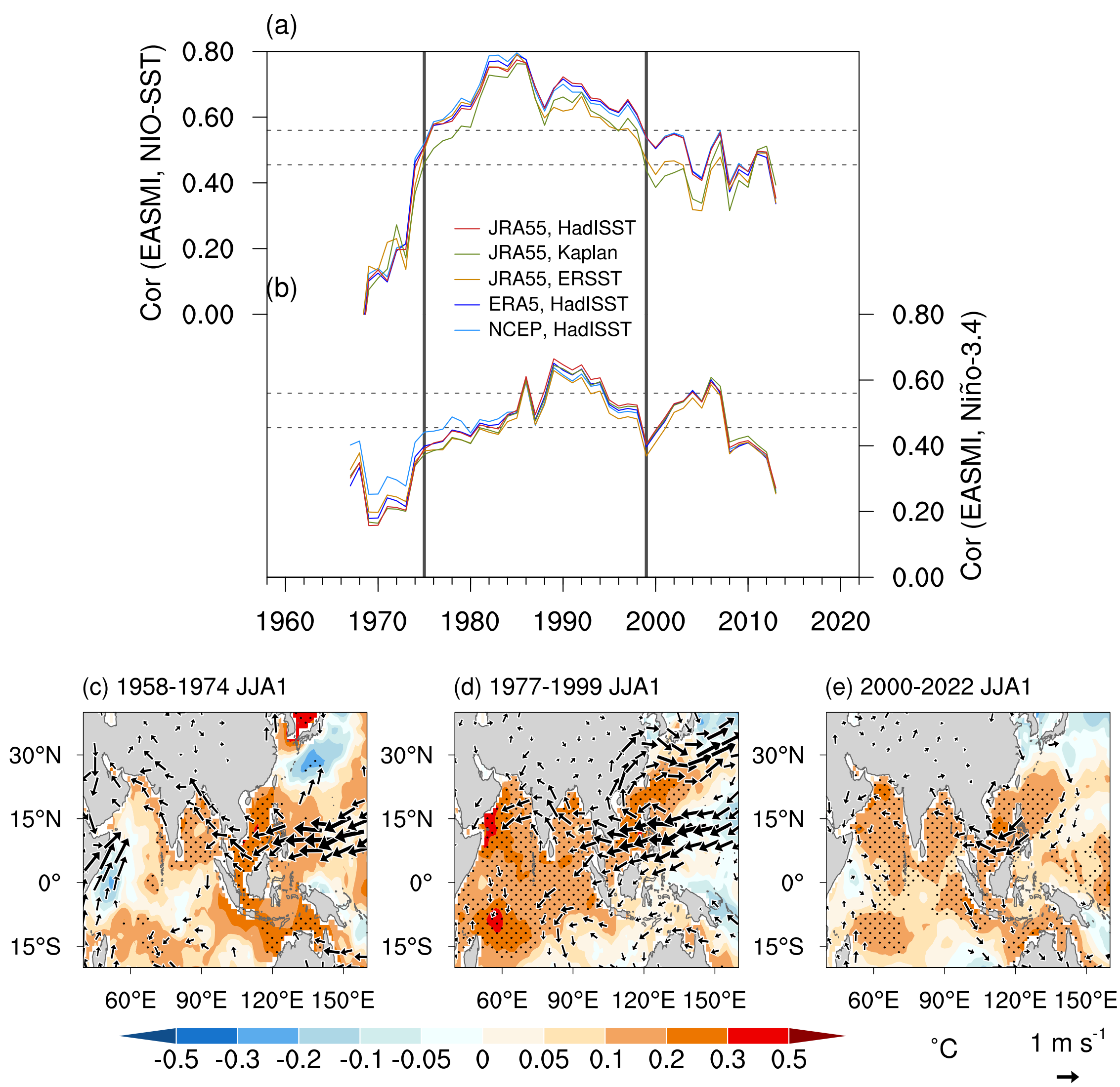

Fig. 1 | Recent interdecadal changes in the impacts of ENSO on the EASM. **a**, **b** The 19-yr sliding correlation between the (**a**) JJA(1) mean EASMI and NIO-SST index over the region (0°–25°N, 40°–100°E), and (**b**) JJA(1) mean EASMI and DJF(0) mean Niño-3.4 index. The dashed lines denote the 99% and 95% confidence levels, and the black lines indicate 1975 and 1999. **c**–**e** SST anomalies (shading) and 850-hPa wind anomalies (vectors) regressed onto the Niño-3.4 index in preceding winter during (**c**) 1958–1974, (**d**) 1977–1999, and (**e**) 2000–2022. SST anomalies exceeding the 95% confidence level are dotted, and only significant wind anomalies are shown.

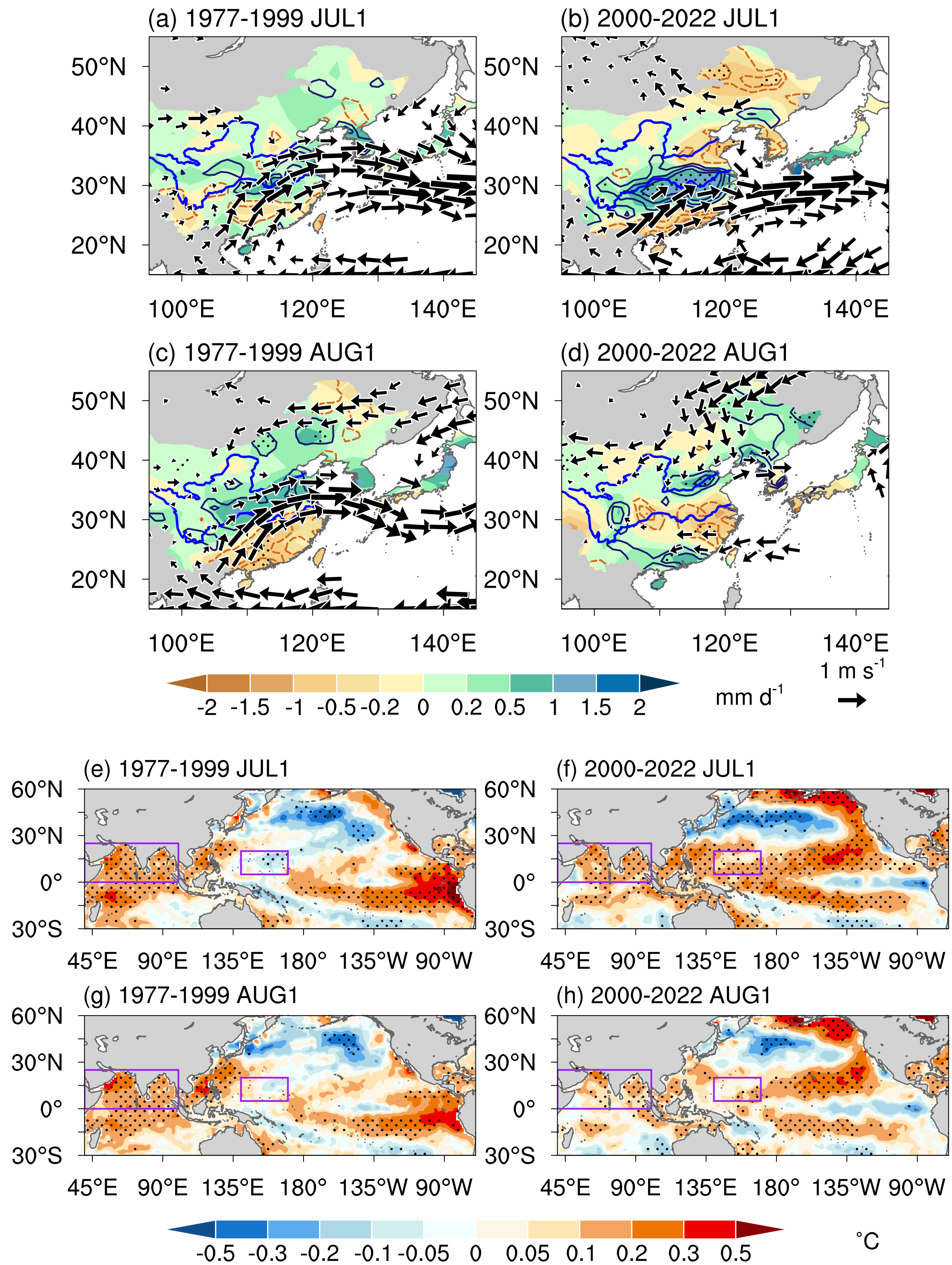

Fig. 2 | SST, wind, and rainfall anomalies associated with the preceding ENSO. **a**–**d** Rainfall (shading) and 850-hPa wind anomalies (vectors) in July(1) and August(1) regressed onto the Niño-3.4 index in preceding winter during (**a**), (**c**) 1977–1999 and (**b**), (**d**) 2000–2022. Station rainfall anomalies in China are plotted in contours (10 mm m^{-1} intervals with zero omitted). Here, the CMAP rainfall anomalies start in 1979 owing to the data availability. **e**–**h** as in (**a**–**d**), but for SST anomalies (shading). The boxes denote the NIO (0°–25°N, 40° – 100°E) and WNP (5°–20°N, 140°–170°E) regions, respectively. SST and rainfall anomalies exceeding the 95% confidence level are dotted, and only significant wind anomalies are shown.

response is confirmed by the summertime [June–August (JJA)] wind anomalies associated with the preceding winter ENSO (Fig. 1d, e).

The EASM has a clear intra-seasonal variation that cannot be fully reflected in the summer mean timescale[57]. On close inspection, around the early 2000s, the EASM shows noticeable interdecadal changes in August (Fig. 2a–d). During 1977–1999, positive rainfall anomalies mainly occurred over the Yangtze and Huaihe River valleys of China, Korea, and Japan, and negative anomalies appeared over southern China in July (Fig. 2a). The WNPAC, with the southerly wind anomalies, brings plentiful water vapor to the region from central China around the Yangtze and Huaihe River basins to Japan, contributing to the wet conditions there. The August rainfall anomalies are similar to those in July but shift slightly northward owing to the northward advance of WNPAC (Fig. 2c). However, during 2000–2022, the evolution of rainfall anomalies shows distinct features among individual months. The positive rainfall anomalies in July extend along the Yangtze River valley of China and the south coast of Japan, and negative anomalies occur over the coastal regions of southern China (Fig. 2b). In contrast, in August, the anomalous rainfall pattern is generally opposite to that in July, displaying dry conditions from the Yangtze River basin to the south coast of Japan, and wet conditions in the coastal regions of southern China (Fig. 2d). This evolution of the rainfall anomalies from July to August is associated with the dramatic change in the WNPAC whereby it quickly disintegrates and changes to an anomalous cyclone in August. Meanwhile, the rainfall anomalies in North China change from negative to positive values, which may be related to the mean-state precipitation[58,59]. The three possible outliers of summer extreme events, 1998, 2020, and 2022, do not influence the conclusion. Therefore, the rapid decay of the WNPAC is found to be the key factor controlling the weak response of EASM rainfall in August since the early 2000s.

Interdecadal change in the ENSO-induced TIO responses

The ENSO-induced NIO SST warming exerts significant support to the summertime WNPAC and then the EASM[21,22,32]. Around the early 2000s, the characteristics of the SST anomalies in the NIO experienced obvious interdecadal changes (Fig. 2e–h). During 1977–1999, there is prominent warming in the NIO, together with marked cooling in the WNP and warming in the tropical central-eastern Pacific in July (Fig. 2e). In August, the SST anomalies over the WNP and central-eastern Pacific gradually decay, with a relatively weak amplitude (Fig. 2g). Instead, the NIO SST warming robustly persists, which is responsible for the long-lasting maintenance of the WNPAC in August (Fig. 2c). Specifically, the NIO warming generates strong positive rainfall anomalies, which trigger an atmospheric Matsuno–Gill pattern in the tropospheric temperature that increases as a result of forced atmospheric Kelvin waves (Fig. S1a, e). The warm Kelvin waves penetrate into the tropical western Pacific, inducing Ekman divergence in the WNP to suppress convection, which maintains the WNPAC in August (Fig. S1a, c, e).

However, during 2000–2022, the pattern of SST anomalies differs conspicuously from that during 1977–1999, featuring much weaker NIO warming shrinking northward in July and dramatically decaying in August (Fig. 2f, h). Meanwhile, the warm SST anomalies over the central-eastern Pacific decay quickly, accompanied by the absence of the cold SST anomalies over the WNP (Fig. 2f, h). In August, the fast-decaying NIO warming cannot sustain the WNPAC. The atmospheric Matsuno–Gill response over the TIO is negligible, which leads to the change over the WNP from anticyclonic to cyclonic circulation anomalies in August (Fig. S1b, d, f).

In Fig. 2, SST anomalies over the three key regions—that is, the tropical central-eastern Pacific, NIO, and WNP—experience apparent interdecadal changes. To illustrate the changing influences of such tropical anomalous SSTs on the EASM, the lead–lag correlation coefficients of the EASM index (EASMI) with SST anomalies in the Niño-3.4, NIO, and WNP regions during 1958–2022 are further examined (Fig. 3). During 1958–1974, SST anomalies in the Niño-3.4, NIO, and WNP regions all insignificantly correlate with the EASMI (Fig. 3a). After the ENSO mature winter, the NIO SST rapidly decays, which exerts no effect on the EASM. This is because the fast decaying ENSO switches its phase in the following mid-spring, which is unable to support the summertime NIO SST via ocean–atmosphere feedback over the TIO[31,36,38].

By contrast, during 1977–1999, the significant positive correlation between the EASMI and NIO-SST index displays a broad peak from the preceding winter to summer, indicating the strong influence of NIO SST on the EASM (Fig. 3b), consistent with previous findings[36,38]. The EASMI has a strong positive and negative correlation with the Niño-3.4 index in preceding and following seasons, corresponding to the ENSO cycle. The slowly decaying tropical central-eastern Pacific SST, with its phase persisting to the following summer, excites strong positive feedback within the TIO (Fig. 4a, c, e, g). Besides, the negative correlation between the EASMI and the WNP-SST index is enhanced compared to that during 1958–1974 (Fig. 3a, b). According to previous research[14,26,27,45,54], the strengthened WNP SST in response to ENSO, also remotely supports the positive feedback via interbasin air–sea coupling in the ENSO decaying phase (Fig. 4a, c, e, g). Such a strengthened TIO response develops and maintains the NIO SST warming (Fig. 2e, g), which directly sustains the WNPAC (Fig. 2a, c).

During 2000–2022, however, the positive correlation between the EASMI and NIO-SST index becomes weak and peaks twice in the preceding winter and early summer, indicating a weakening of the NIO impact on the EASM (Fig. 3c). The correlation between the EASMI and Niño-3.4 index weakens during 2000–2022. ENSO decays earlier than during 1977–1999, which could only force weak ocean–atmosphere feedback within the TIO (Fig. 4b, d, f, h), resulting in the weak summer peak in the NIO (Fig. 2f, h). Additionally, the negative correlation between the EASMI and WNP-SST index weakens (Fig. 3c). The ENSO-induced weak WNP SST[45,54] may contribute to the weak NIO feedback in the ENSO decaying phase (Fig. 4b, d, f, h). The resultant weak NIO warming rapidly decays and fails to maintain the WNPAC in August (Fig. 2d, h).

Therefore, the ocean–atmosphere feedback over the TIO varies during 1958–2022, which plays a key role in the response of the EASM to ENSO's interdecadal changes. For the change around the mid-1970s, the WNP SST helps intensify the ENSO-induced positive feedback over the TIO during 1977–1999[14,38]. In contrast, the ENSO-induced TIO feedback weakens during 2000–2022, forcing weaker summertime NIO SST compared to that during 1977–1999. Besides, the WNP SST also weakens, which may be another factor contributing to the weak NIO SST during 2000–2022.

The role of WNP air–sea coupling

Different paces of ENSO decay can result in diverse responses over the TIO, with different impacts on the EASM[36,38,45]. Additionally, we found that the WNP air–sea coupling potentially played an important role in changing the NIO feedback around the early 2000s. To verify the above hypothesis, we thus classified ENSO events into two groups—namely, slowly decaying ENSOs with strong WNP SST (SD-SWNP) anomalies, and fast-decaying ENSOs with weak WNP SST (FD-WWNP) anomalies. For the period of 1958–2022, the number of SD-SWNP (FD-WWNP) cases is the most (least) during 1975–1999 and the least (most) during 1958–1974, which suggests the selected cases also experienced interdecadal changes around the mid-1970s and early-2000s (Table 1). This interdecadal change in the pace of ENSO is consistent with the shift in ENSO's period revealed in previous studies[42,56,60].

The TIO responses to SD-SWNP and FD-WWNP exhibit remarkable differences (Fig. 5). For the SD-SWNP cases, the ENSO-excited strong feedback in the TIO forces strong southwest Indian Ocean warming, inducing wind anomalies across the equator from the decaying spring (Fig. 5a). The wind anomalies turn northeasterly over the NIO owing to the Coriolis effect, which intensify the climatological northeast monsoon and cool the local SST[30,61]. After the summer monsoon onset in May, the anomalous northeasterly winds turn into a warming effect on the NIO by weakening the southwest monsoon[31]. In this case, the NIO SST warming persists significantly through the decaying summer (Fig. 5a). By contrast, for the FD-WWNP cases, the ocean–atmosphere feedback over the TIO is quite weak, resulting in the roughly symmetrical SST anomalies along the equator (Fig. 5b). The wind anomalies over the NIO disintegrate during the decaying spring, which induce the fast decaying of NIO warming. We also compared the TIO responses to SD-SWNP and the slowly decaying ENSOs without the effect of WNP SST (SD) (Fig. S2). The SD leads to a weaker TIO response than SD-SWNP, inducing weaker and shorter-lasting NIO warming from the decaying summer (Fig. S2). Hence, the WNP air–sea coupling is a key factor determining the changes in the ENSO-induced NIO feedback.

From the IPOC perspective, the WNP SST could also influence the NIO feedback during the decaying spring, through enhancing easterly winds extending from the WNP to the NIO. For the SD-SWNP cases, the anomalous diabatic cooling over the WNP forces the WNPAC via a cold

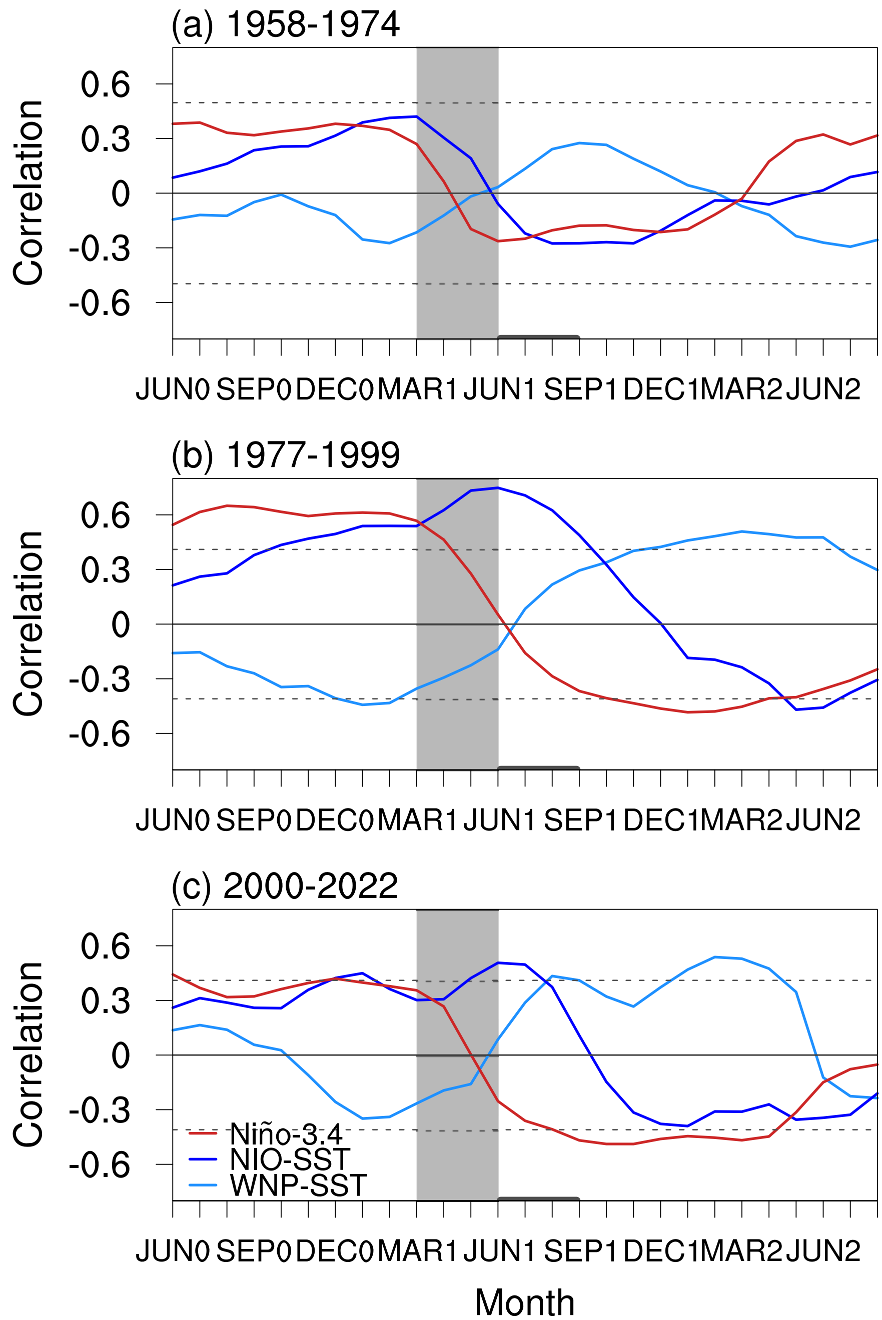

Fig. 3 | Correlations of the EASM with ENSO, NIO, and WNP SSTs. Lead–lag correlations of the JJA(1) mean EASMI with Niño-3.4 index, NIO-SST index, and WNP-SST index during (**a**) 1958–1974, (**b**) 1977–1999 and (**c**) 2000–2022. The dashed lines denote the 95% confidence level. The gray shading indicates ENSO decaying spring [March(1) to May(1)], and the gray line at the bottom indicates decaying summer [June(1) to August(1)].

Rossby wave response (Fig. 6a, c, e). The anomalous easterly winds on the southern flank of the WNPAC extend into the NIO, reinforcing the local northeasterlies. The easterly wind response over the NIO weakens the climatological westerlies and reduces the latent heat flux loss from the ocean, thus developing the NIO to warm (Fig. 6a, c, e). However, for the FD-WWNP cases, the wind anomalies are not well organized in space and are accompanied by the absence of the WNP SST cooling (Fig. 6b, d, f). The easterly wind response over the NIO is quite weak, which further leads to the fast decaying of NIO warming.

Model verification

To verify the mechanism of the interdecadal change around the early 2000s, we analyze the Atmospheric Model Intercomparison Project (AMIP) experiments in 44 CMIP6 (phase 6 of the Coupled Model Intercomparison Project) models from 1979 to 2014. Similar to the analyses based on observations, we calculated the 19-yr sliding correlations between the EASMI and the preceding Niño-3.4 index in the models (Fig. 7a). The majority of models can simulate a positive correlation between the EASM and NIO SST during 1980–1999, with 41 of them showing a weaker relationship during 2000–2014 than during 1980–1999 (Fig. 7b), and these 41 CMIP6 AMIP models are further selected (bold typeface in Table S1). Although the multi-model ensemble mean of the correlation between the EASMI and Niño-3.4 index in the selected 41 models is weak relative to the observation, it successfully captures the weakened relationship since the early 2000s (Fig. 7a). The regression results for the selected 41 CMIP6 AMIP models are then calculated (Fig. 8a–d). Compared to 1980–1999 (Fig. 8a, c), the SST anomalies over the central-eastern Pacific dramatically decay, and the cold SST over the WNP is much weaker in July and August, accompanied by the fast decaying NIO warming during 2000–2014 (Fig. 8b, d). The resultant wind anomalies change to a cyclonic circulation and suppress the northward transportation of water vapor from the ocean, indicating a weakened EASM response during 2000–2014 (Fig. 8b, d). Although the

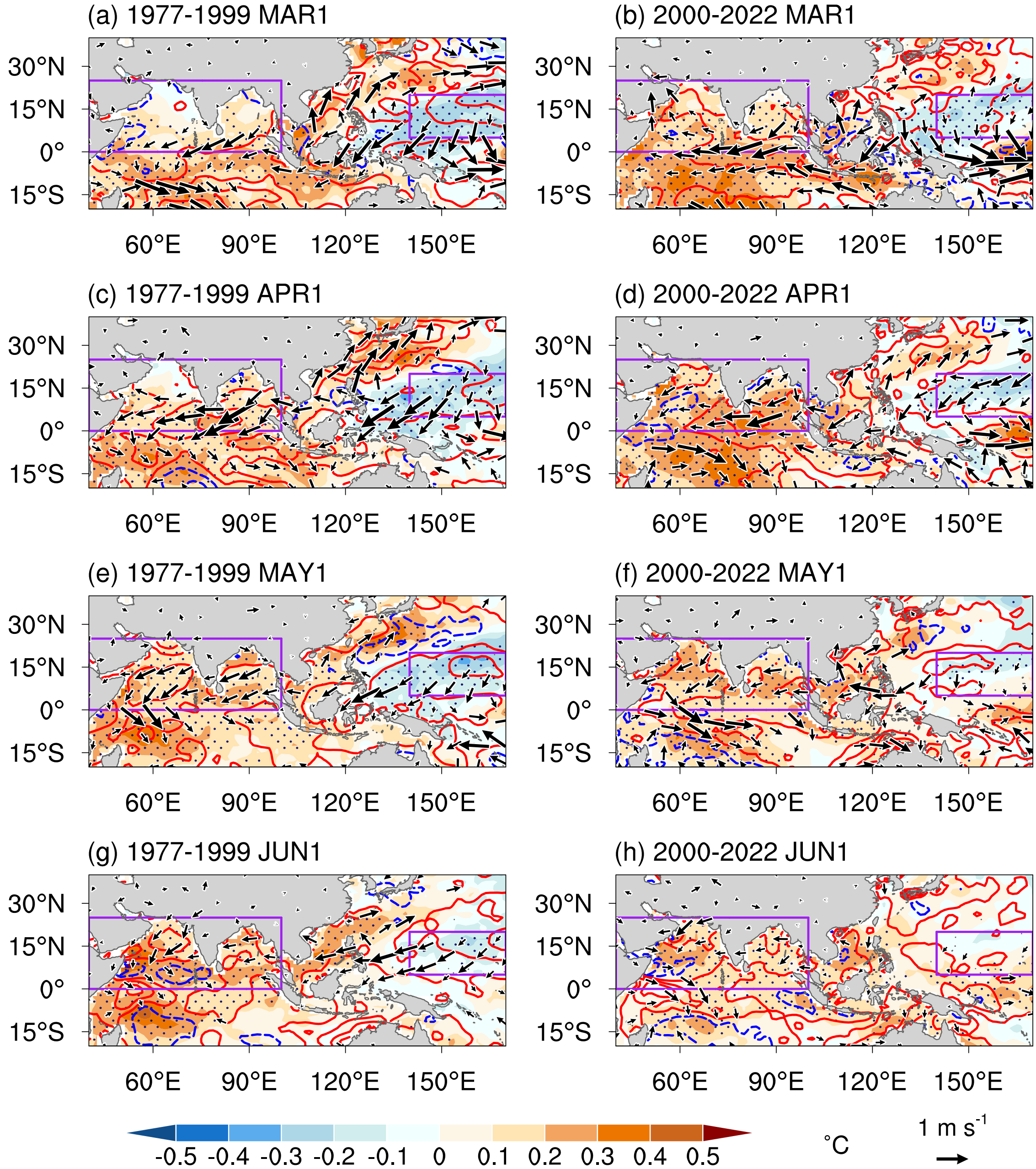

Fig. 4 | SST, wind, and heat flux anomalies associated with the preceding ENSO. SST anomalies (shading), 10 m wind anomalies (vectors), and surface latent heat flux anomalies (contours; 5 W m^{-2} intervals with zero omitted) regressed onto the Niño-3.4 index in preceding winter during (**a**), (**c**), (**e**), (**g**) 1977–1999 and (**b**), (**d**), (**f**), (**h**) 2000–2022 from March(1) to June(1). The boxes denote the NIO (0°–25°N, 40° − 100°E) and WNP (5°–20°N, 140°–170°E) regions, respectively. SST anomalies exceeding the 95% confidence level are dotted, and only significant wind anomalies are shown.

AMIP models simulate the change in wind anomalies one month early, the models nevertheless capture the main features of the difference in the summer atmospheric response to the SST anomalies between 1980–1999 and 2000–2014.

The eastern Pacific pacemaker experiments based on the Community Earth System Model, version 2.1.2 (CESM2.1.2) are further analyzed to verify the role of the tropical Pacific SST (See Methods for details of model settings). In the pacemaker experiments, only the variations in the evolution of ENSO-related SST anomalies in the eastern Pacific are included. There are 7 out of 10 members that successfully simulate the weakening of the EASM and ENSO relationship after 1999 as observed (Fig. 7c). The ensemble mean regression for the selected members produces different summer SST anomalies between 1980–1999 and 2000–2019 (Fig. 8e–h). Additionally, the difference in the coupled mode within the TIO and WNP can be well captured in the CESM2.1.2 pacemaker experiments. During 2000–2019, the tropical Pacific SST warming decayed faster and the WNP SST cooling is weaker (Fig. 8f, h) than that during 1980–1999 (Fig. 8e, g), which can only force weak ocean–atmosphere feedback and NIO warming, resulting in a weaker summertime WNPAC. Similar to the observed analyses, we also checked the 19-year sliding correlations between the EASM and NIO SST in the models (Fig. S3). There are 35 out of 44 CMIP6 AMIP models and 7 out of 10 CESM members that capture the weaker relationship during 2000–2014 than during 1980–1999 as observed. In conclusion, these results from the CMIP6 AMIP and CESM2.1.2 pacemaker experiments support the observational results that the ENSO-related weak ocean–atmosphere feedback, which extends beyond the TIO and involves

Table 1 | Definitions of SD-SWNP and FD-WWNP, and corresponding selected years for the period 1958–2022

Types		Definitions	1958–1974	1975–1999	2000–2022
SD-SWNP	El	DJF Niño-3.4 > 0.5 JJA Niño-4 > 0 MAM WNP < -0.4	1965/66	1976/77, 1979/80, 1986/87, 1991/92	2014/15, 2015/16
	La	DJF Niño-3.4 < −0.5 JJA Niño-4 < 0 MAM WNP > 0.4	1970/71	1983/84, 1988/89, 1995/96, 1998/99	1999/2000, 2007/08, 2010/11, 2020/21
FD-WWNP	El	DJF Niño-3.4 > 0.5 JJA Niño-4 < 0 MAM WNP > -0.4	1963/64, 1969/70	1987/88	2006/07
	La	DJF Niño-3.4 < −0.5 JJA Niño-4 > 0 MAM WNP < 0.4	1964/65, 1967/68, 1971/72	1985/86	2005/06, 2008/09,

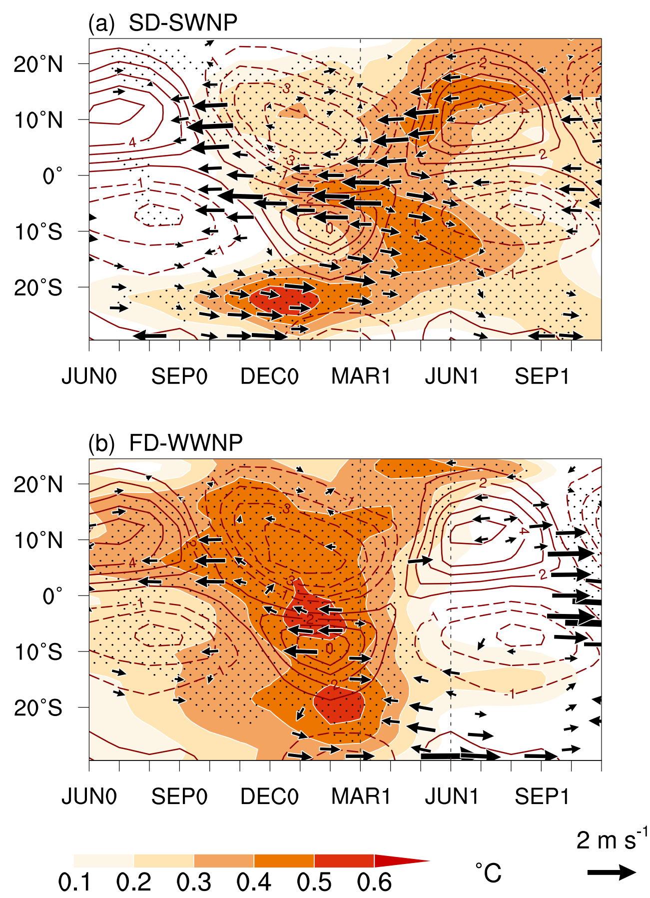

Fig. 5 | Evolutions of composite SST and wind anomalies in the TIO for SD-SWNP and FD-WWNP groups. Time–latitude section of the composite differences of SST anomalies (shading) and 10 m wind anomalies (vectors) averaged over the TIO (40°–100°E) between El Niño and La Niña cases for (**a**) SD-SWNP and (**b**) FD-WWNP. The zonal 10 m wind climatology is plotted in contours (1 m s^{-1} intervals with zero omitted). SST anomalies exceeding the 95% confidence level are dotted, and only significant wind anomalies are shown.

the WNP, has played a decisive role in the weakened EASM response since the early 2000s.

Discussion

In this study, we found that the influence of ENSO on the EASM has changed since the early 2000s, showing a weakened EASM response. Also, we revealed that this interdecadal weakening of ENSO's impact is linked to the changes in ENSO's rate of decay around the early 2000s. Consistent with the IPOC effect, the ENSO-excited ocean–atmosphere feedback in the TIO varies over the past few decades, which directly forces the changing responses of the EASM to ENSO. Here, we highlight that, in the ENSO decaying phase, the WNP air–sea coupling played a crucial role in changing the NIO feedback around the early 2000s.

During 1977–1999, ENSO decays slowly, with its phase persisting to the following summer, thereby triggering strong positive feedback within the TIO. The WNP SST anomalies also remotely support the positive feedback via inter-basin air–sea interaction. The anomalous diabatic cooling over the WNP forces the WNPAC through a Rossby wave response. The anomalous easterlies on the southern flank of the WNPAC extend into the NIO, reinforcing the local northeasterlies and contributing to the NIO warming via positive WES feedback. The resultant NIO SST anomalies develop and robustly persist through the decaying summer, directly maintaining the summertime WNPAC. The long-lasting WNPAC further generates positive rainfall anomalies from central China around the Yangtze and Huaihe River basins to Japan, and negative anomalies over southern China in August.

However, during 2000–2022, ENSO decays earlier than during 1977–1999, which can only force weak ocean–atmosphere feedback within the TIO, resulting in a weak summer peak in the NIO. In addition, the WNP SST anomalies warm up, which contributes to the weak NIO SST anomalies owing to the collapse of the easterly wind response. In turn, this weak NIO warming rapidly decays, which cannot sustain the WNPAC in August. The circulation anomalies over the WNP change to a cyclonic circulation, generating negative rainfall anomalies from the Yangtze River basin to the south coast of Japan, and positive anomalies in the coastal regions of southern China in August. The mechanism is well supported by the results of the CMIP6 AMIP and CESM2.1.2 pacemaker simulations.

This study demonstrates that the EASM response to ENSO has weakened significantly in August since the early 2000s, which can be largely explained by the fast decaying of ENSO and the resultant weakened ocean–atmosphere feedback extending beyond the TIO and involving the WNP, shedding light on the IPOC effect. It carries important implications for the prediction of the EASM and the adaptation to climate change. It should be noted that the ENSO is a complex phenomenon and all these properties—period, amplitude, spatial structure, and temporal evolution of ENSO events—may not be mutually independent. Here, we emphasized the dominant role of ENSO period in the Indo-western Pacific air-sea coupling during the decaying summer, while weak ENSO tends to excite a weak ENSO teleconnection to the Indo-western Pacific region[14,33,46,53]. Besides, ENSO's impact on the EASM may also involve other factors that are not considered here, especially the Atlantic SST[5,62–68]. The Atlantic SST can potentially have an ENSO-related influence on the EASM in subsequent seasons despite being distant from East Asia[69–75]. We only focus on the factors affecting the ENSO-EASM relationship from the perspective of ENSO, while the impacts of non-ENSO factors may also contribute to the relationship[6,76–78] and deserve further investigation in future.

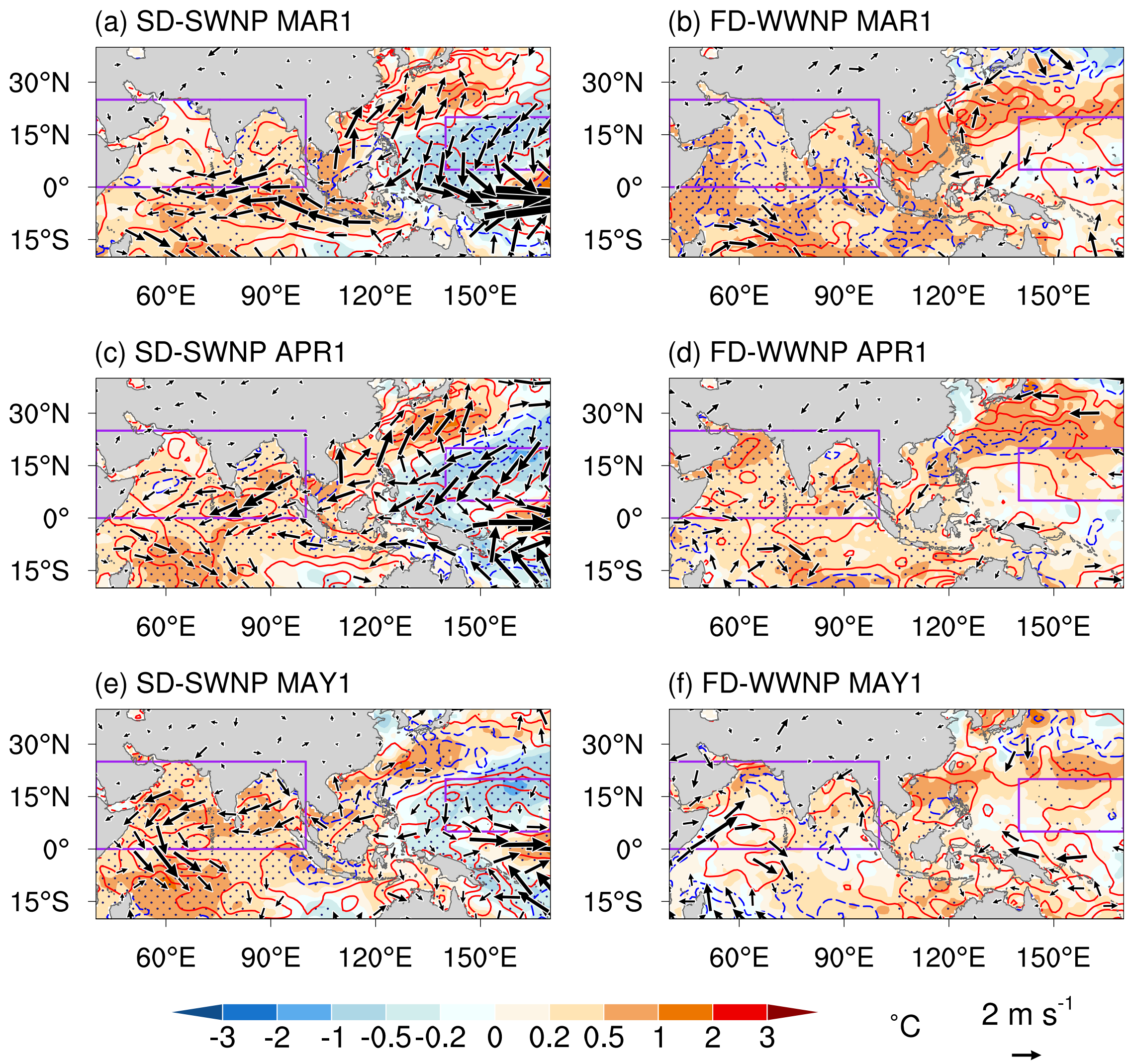

Fig. 6 | Composite SST, wind, and heat flux anomalies for SD-SWNP and FD-WWNP groups. Composite differences of SST anomalies (shading), 10 m wind anomalies (vector) and surface latent heat flux anomalies (contours; 10 W m^{-2} intervals with zero omitted) between El Niño and La Niña cases for (**a**), (**c**), (**e**) SD-SWNP and (**b**), (**d**), (**f**) FD-WWNP from March(1) to May(1). The boxes denote the NIO (0°–25°N, 40° − 100°E) and WNP (5°–20°N, 140°–170°E) regions, respectively. SST anomalies exceeding the 95% confidence level are dotted, and only significant wind anomalies are shown.

Methods

Observational datasets

Monthly mean atmospheric reanalysis data were derived from the JRA-55 dataset developed by the Japan Meteorological Agency[79], which has a horizontal resolution of 1.25° × 1.25°, is available since 1958, and is more suitable than other reanalyzes for studying the interannual variability in East Asia[80]. The National Centers for Environmental Prediction (NCEP)–Department of Energy atmospheric reanalysis[81] and the fifth generation European Centre for Medium-Range Weather Forecasts reanalysis (ERA5) data[82] were also used, and the related results verify the conclusions based on JRA-55. Monthly mean SST data are from the Hadley Centre Sea Ice and Sea Surface Temperature dataset, which has a horizontal resolution of 1°× 1° and is available from 1870 to the present day[83]. And the results were verified by the Extended Reconstructed SST dataset, version 5 (ERSST.v5)[84], and the Kaplan SST[85]. The monthly precipitation data are from the China Meteorological Administration's 160-station precipitation dataset available from 1951, and the Climate Prediction Center Merged Analysis of Precipitation (CMAP) dataset[86] at a horizontal resolution of 2.5° × 2.5° and covering from 1979 to the present day. Additionally, this study employed monthly mean net surface heat flux from the Objectively Analyzed Air–Sea Fluxes dataset[87] at a horizontal resolution of 2.5° × 2.5° from 1958 to 2022. In this study, positive (negative) flux anomalies indicate that the ocean gains (gives) heat from (to) the atmosphere. This study focuses on the period 1958–2022, and anomalies for all variables were computed as the deviations from the climatological mean over the entire period, except for those of CMAP, which started in 1979 owing to the data availability. All the data have been detrended to remove possible influences of global warming. Based on the sliding correlation between the EASM and NIO SST, we select two equal sub-periods, 1977–1999 and 2000–2022, to compare the changing role of ENSO. Statistical significance was determined using the two-tailed Student's *t*-test. The numerals after months denote the ENSO developing (0) and decay (1) years.

Definitions of climate indices

A widely used EASMI[88] was selected to depict the intensity of the EASM, which is calculated as the difference in the summer mean [June–August (JJA)] 850-hPa zonal winds between the regions of (5–15°N, 90–130°E) and (22.5–32.5°N, 110–140°E), but with the sign reversed. This index can capture well the dominant mode of the EASM and is highly correlated with the

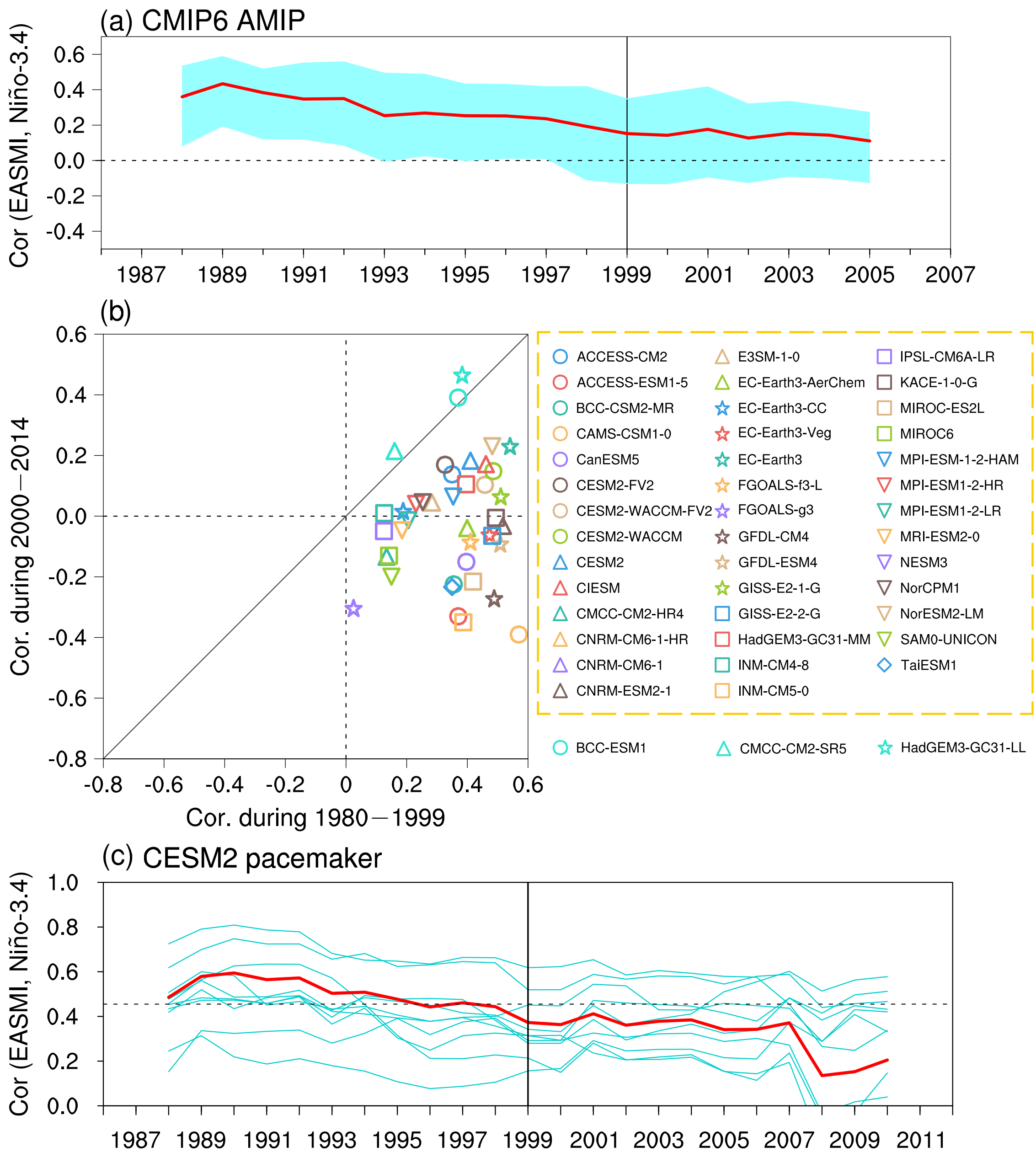

Fig. 7 | Weakened impacts of ENSO on the EASM in the CMIP6 AMIP and CESM2.1.2 pacemaker simulations. a The 19-yr sliding correlation between the DJF(0) mean Niño-3.4 index and JJA(1) mean EASMI in CMIP6 AMIP models. The shading indicates the 10th and 90th percentiles of 44 CMIP6 AMIP models. The red line represents the multi-model ensemble mean of 41 selected models, and the black line indicates 1999. **b** Scatterplot of the Niño-3.4 and EASM correlation coefficients between the periods of 1980–1999 and 2000–2014 for the 44 CMIP6 AMIP models. The solid grey line is the critical line where the correlation coefficients of the two periods are equal. The correlation coefficients of the models inside the yellow dashed rectangular box during 1980–1999 are positive and greater than in the period 2000–2014. **c** as in (**a**), but for the CESM2.1.2 pacemaker experiments. The blue lines represent the results for 10 members of the CESM2.1.2 pacemaker experiments, and the red line represents the ensemble mean of 7 selected members. The dashed line denotes the 95% confidence level.

Niño-3.4 index—more so than with the other indices[89]. The Niño-3.4 index was used to represent ENSO variability, which is defined as the SST anomalies averaged over the region (5°S–5°N, 170°–120°W). In this study, we mainly consider the symmetric response to ENSO for convenience. The asymmetric response to ENSO was also examined (Fig. S4), revealing that the responses to El Niño are roughly opposite to those of La Niña, though not antisymmetric[90–92]. The NIO SST index was defined as the anomalous SST averaged over the region (0°–25°N, 40°–100°E), and the WNP SST index was represented by the anomalous SST averaged over (5°–20°N, 140°–170°E).

This study classified ENSO events into two groups (i.e., SD-SWNP and FD-WWNP) to verify the role of WNP air–sea coupling in changing the NIO feedback around the early 2000s. ENSO events were identified by the winter mean [December–February (DJF)] normalized Niño-3.4 index being greater than 0.5 or less than −0.5. Consistent with a previous study[60], the summer (JJA) mean normalized Niño-4 index was selected to further classify the slowly decaying and fast decaying ENSO cases, which is defined by the SST anomalies averaged over the region (5°S–5° N, 160°E–150°W). The intensity of WNP SST anomalies was quantified by the spring mean [March–May (MAM)] normalized WNP SST index. The above three indices were used to distinguish and select the SD-SWNP and FD-WWNP cases, with the definitions and cases shown in Table 1. The composite results were based on El Niño minus La Niña.

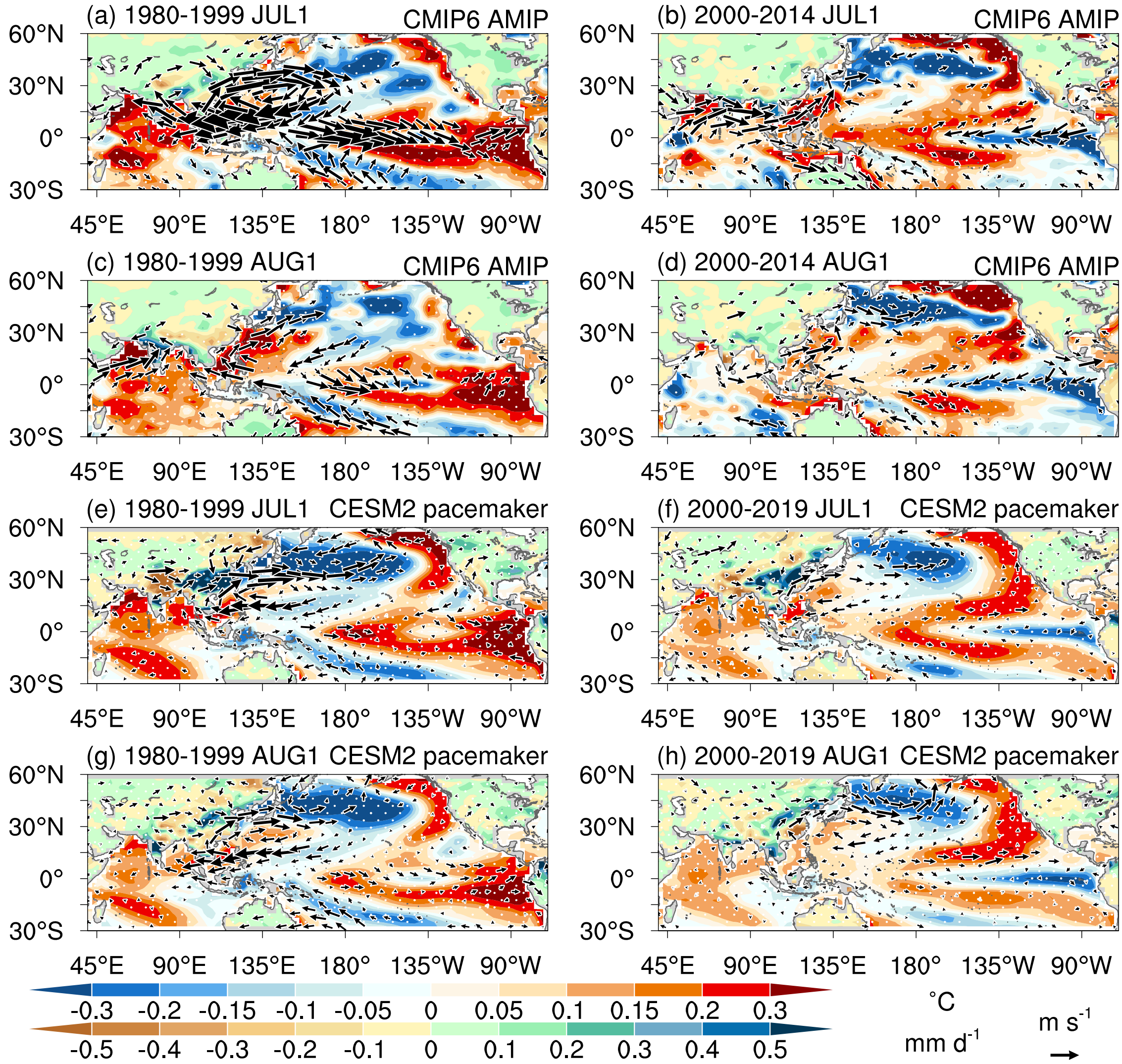

Fig. 8 | CMIP6 AMIP and CESM2 pacemaker simulations. a–d The multi-model ensemble mean of 41 selected CMIP6 AMIP models for the 850 hPa wind anomalies (vectors; 0.5 m s^{-1}), SST and rainfall anomalies (shading) regressed onto the preceding Niño-3.4 index in (**a**), (**b**) July(1) and (**c**), (**d**) August(1) during (**a**), (**c**) 1980–1999 and (**b**), (**d**) 2000–2014. **e**–**h** as in (**a**–**d**), but for the 7 selected members of the CESM2.1.2 pacemaker experiments for the 850 hPa wind anomalies (vectors; 1 m s^{-1}), SST and rainfall anomalies (shading) in (**e**), (**f**) July(1) and (**g**), (**h**) August(1) during (**e**), (**g**) 1980–1999 and (**f**), (**h**) 2000–2019. Dots and arrows indicate regions where more than 70% of models agree on the sign.

Models

The simulations from the AMIP models participating in CMIP6[93] were employed to confirm the mechanism of the weakened EASM response since the early 2000s. The 44 CMIP6 AMIP models are listed in Table S1. A 10-member Pacific Pacemaker experiment[94] for the period 1880–2019 was also analyzed to verify the role of the Pacific SST, which was conducted by CESM2.1.2. In the CESM2 Pacific Pacemaker Ensemble, time-evolving SST anomalies in the eastern tropical Pacific were nudged toward the observations. In this way, the observed evolution of ENSO was maintained in each simulation (i.e., ENSO was the pacemaker), with the rest of the model's coupled climate system free to evolve. All the model data were bilinearly interpolated onto a 2.5° × 2.5° grid before analysis. The ensemble mean was calculated by averaging the variables in all the selected models with equal weight.

Data availability

Data relevant to this paper can be downloaded from the websites listed below: JRA-55 provided by the Japan Meteorological Agency at https://climatedataguide.ucar.edu/climate-data/jra-55; NCEP-DOE provided by the National Centers for the Environmental Prediction-Department at https://psl.noaa.gov/data/gridded/data.ncep.reanalysis2.html; ERA5 provided by the European Centre for Medium-Range Weather Forecasts at https://www.ecmwf.int/en/forecasts/datasets/reanalysis-datasets/era5; HadISST provided by the Met Office Hadley Centre at https://www.metoffice.gov.uk/hadobs/hadisst/; ERSST provided by the US National Oceanic and Atmospheric Administration at https://www1.ncdc.noaa.gov/pub/data/cmb/ersst/v5/netcdf/; Kaplan SST provided by the NOAA PSL, Boulder, Colorado, USA, at http://psl.noaa.gov/data/gridded/data.kaplan_sst.html; 160-station precipitation data from the Chinese Meteorology Administration at http://www.ncc-cma.net/; CMAP provided by the Climate Prediction Center at https://psl.noaa.gov/data/gridded/data.cmap.html; OAFlux supported by the Woods Hole Oceanographic Institution at https://oaflux.whoi.edu/data-access/; CMIP6 models are publicly available at https://esgf-node.llnl.gov/search/cmip6/; CESM2 pacemaker experiments provided by the Climate Variability and Change Working Group at https://www.cesm.ucar.edu/working-groups/climate.

Code availability

The data in this study were processed and plotted by the NCAR Command Language (NCL). Codes used in this study are available from the corresponding author upon request.

Received: 24 October 2024; Accepted: 25 February 2025;
Published online: 20 March 2025

References

1. Zhang, R., Sumi, A. & Kimoto, M. Impact of El Niño on the East Asian monsoon: a diagnostic study of the '86/87 and '91/92 events. *J. Meteorol. Soc. Japan* **74**, 49–62 (1996).
2. Chang, C. P., Zhang, Y. & Li, T. Interannual and interdecadal variations of the East Asian summer monsoon and tropical pacific SSTs. Part II: meridional structure of the monsoon. *J. Clim.* **13**, 4326–4340 (2000).
3. Wang, B., Wu, R. & Fu, X. Pacific-East Asian teleconnection: how does ENSO affect East Asian climate? *J. Clim.* **13**, 1517–1536 (2000).
4. Li, T. et al. Theories on formation of an anomalous anticyclone in western North Pacific during El Niño: a review. *J. Meteorol. Res.* **31**, 987–1006 (2017).
5. Zhang, R. H., Min, Q. Y. & Su, J. Z. Impact of El Niño on atmospheric circulations over East Asia and rainfall in China: Role of the anomalous western North Pacific anticyclone. *Sci. China Earth Sci.* **60**, 1124–1132 (2017).
6. Zhou, Z. Q., Xie, S. P. & Zhang, R. Historic Yangtze flooding of 2020 tied to extreme Indian Ocean conditions. *Proc. Natl. Acad. Sci. USA*. **118**, e2022255118 (2021).
7. Ding, Y., Liu, Y. & Hu, Z. Z. The Record-breaking Mei-yu in 2020 and associated atmospheric circulation and tropical SST anomalies. *Adv. Atmos. Sci.* **38**, 1980–1993 (2021).
8. He, J., Ju, J., Wen, Z., Lü, J. & Jin, Q. A review of recent advances in research on Asian monsoon in China. *Adv. Atmos. Sci.* **24**, 972–992 (2007).
9. Huang, R., Chen, J., Wang, L. & Lin, Z. Characteristics, processes, and causes of the spatio-temporal variabilities of the East Asian monsoon system. *Adv. Atmos. Sci.* **29**, 910–942 (2012).
10. Ding, Y. et al. On the characteristics, driving forces and inter-decadal variability of the East Asian Summer monsoon. *Chin. J. Atmos. Sci.* **42**, 533–558 (2018).
11. Chen, W., Yu, T., Feng, J., Chen, S. & Piao, J. Progress in the study of the impacts of tropical air–sea interactions on the East Asian Summer monsoon. *Chin. J. Atmos. Sci.* **48**, 160–187 (2024).
12. Zhang, R., Akimasa, S. & Masahide, K. A diagnostic study of the impact of El Niño on the precipitation in China. *Adv. Atmos. Sci.* **16**, 229–241 (1999).
13. Chen, W., Feng, J. & Wu, R. Roles of ENSO and PDO in the link of the east asian winter monsoon to the following summer monsoon. *J. Clim.* **26**, 622–635 (2013).
14. Xie, S. P. et al. Indo-western Pacific Ocean capacitor and coherent climate anomalies in post-ENSO summer: a review. *Adv. Atmos. Sci.* **33**, 411–432 (2016).
15. Hu, K., Xie, S. P. & Huang, G. Orographically anchored El Niño effect on summer rainfall in central China. *J. Clim.* **30**, 10037–10045 (2017).
16. Liu, B., Zhu, C., Jiang, N. & Guo, L. Seasonal evolution of anomalous rainband over east china regulated by sea surface temperature anomalies in the Northern Hemisphere. *J. Clim*. 1–44 https://doi.org/10.1175/jcli-d-20-0398.1 (2021).
17. Huang, R. & Wu, Y. The influence of ENSO on the summer climate change in China and its mechanism. *Adv. Atmos. Sci.* **6**, 21–32 (1989).
18. Alexander, M. A. et al. The atmospheric bridge: the influence of ENSO teleconnections on air-sea interaction over the global oceans. *J. Clim.* **15**, 2205–2231 (2002).
19. Wu, R., Hu, Z. Z. & Kirtman, B. P. Evolution of ENSO-related rainfall anomalies in East Asia. *J. Clim.* **16**, 3742–3758 (2003).
20. Lau, N. C. & Nath, M. J. Atmosphere-ocean variations in the Indo-Pacific sector during ENSO episodes. *J. Clim.* **16**, 3–20 (2003).
21. Yang, J., Liu, Q., Xie, S. P., Liu, Z. & Wu, L. Impact of the Indian Ocean SST basin mode on the Asian summer monsoon. *Geophys. Res. Lett*. **34**, (2007).
22. Xie, S. P. et al. Indian Ocean capacitor effect on Indo-Western Pacific climate during the summer following El Niño. *J. Clim.* **22**, 730–747 (2009).
23. Yang, X., Huang, P., Hu, P. & Wang, Z. Distinct impacts of two types of summer ENSO with different temporal evolutions on the Asian Summer monsoon: role of the tropical indo-western Pacific. *J. Clim*. https://doi.org/10.1175/JCLI-D-22-0 (2023).
24. Hu, K., Huang, G., Xie, S. P. & Long, S. M. Effect of the mean flow on the anomalous anticyclone over the Indo-Northwest Pacific in post-El Niño summers. *Clim. Dyn.* **53**, 5725–5741 (2019).
25. Huang, G. et al. A review about Indian Ocean basin mode and its impacts on East Asian summer climate. *Chin. J. Atmos. Sci.* **40**, 121–130 (2016).
26. Kosaka, Y., Xie, S. P., Lau, N. C. & Vecchi, G. A. Origin of seasonal predictability for summer climate over the Northwestern Pacific. *Proc. Natl. Acad. Sci. Usa.* **110**, 7574–7579 (2013).
27. Wu, B., Li, T. & Zhou, T. Relative contributions of the Indian Ocean and local SST anomalies to the maintenance of the western North Pacific anomalous anticyclone during the El Niño decaying summer. *J. Clim.* **23**, 2974–2986 (2010).
28. Kug, J. S., Kirtman, B. P. & Kang, I. S. Interactive feedback between ENSO and the Indian Ocean in an interactive ensemble coupled model. *J. Clim.* **19**, 6371–6381 (2006).
29. Xiang, B., Wang, B., Yu, W. & Xu, S. How can anomalous western North Pacific Subtropical High intensify in late summer? *Geophys. Res. Lett.* **40**, 2349–2354 (2013).
30. Wu, R., Kirtman, B. P. & Krishnamurthy, V. An asymmetric mode of tropical Indian Ocean rainfall variability in boreal spring. *J. Geophys. Res. Atmos*. **113**, (2008).
31. Du, Y., Xie, S. P., Huang, G. & Hu, K. Role of air-sea interaction in the long persistence of El Niño-induced north Indian Ocean warming. *J. Clim.* **22**, 2023–2038 (2009).
32. Wu, B., Zhou, T. & Li, T. Seasonally evolving dominant interannual variability modes of East Asian climate. *J. Clim.* **22**, 2992–3005 (2009).
33. Wang, B., Yang, J., Zhou, T. & Wang, B. Interdecadal changes in the major modes of Asian-Australian monsoon variability: strengthening relationship with ENSO since the late 1970s. *J. Clim.* **21**, 1771–1789 (2008).
34. Ding, R., Ha, K. J. & Li, J. Interdecadal shift in the relationship between the East Asian summer monsoon and the tropical Indian Ocean. *Clim. Dyn.* **34**, 1059–1071 (2010).
35. Zhou, W., Li, C. & Chan, J. C. L. The interdecadal variations of the summer monsoon rainfall over South China. *Meteorol. Atmos. Phys.* **93**, 165–175 (2006).
36. Huang, G., Hu, K. & Xie, S. P. Strengthening of tropical Indian Ocean teleconnection to the northwest Pacific since the mid-1970s: an atmospheric GCM study. *J. Clim.* **23**, 5294–5304 (2010).
37. An, S. I. & Wang, B. Interdecadal change of the structure of the ENSO mode and its impact on the ENSO frequency. *J. Clim.* **13**, 2044–2055 (2000).
38. Xie, S. P. et al. Decadal shift in El Niño influences on Indo-western Pacific and East Asian climate in the 1970s. *J. Clim.* **23**, 3352–3368 (2010).
39. Cai, W. et al. Changing El Niño–Southern oscillation in a warming climate. *Nat. Rev. Earth Environ.* **2**, 628–644 (2021).
40. Yeh, S. W. et al. El Niño in a changing climate. *Nature* **461**, 511–514 (2009).
41. McPhaden, M. J. A 21st century shift in the relationship between ENSO SST and warm water volume anomalies. *Geophys. Res. Lett*. **39**, (2012).
42. Hu, Z.-Z. et al. The Interdecadal Shift of ENSO Properties in 1999/2000: A Review. *J. Clim.* **33**, 4441–4462 (2020).
43. Chen, W. et al. Recent progress in studies of the variabilities and mechanisms of the East Asian Monsoon in a changing climate. *Adv. Atmos. Sci.* **36**, 887–901 (2019).

44. Chen, W. et al. Recent advances in understanding multi-scale climate variability of the Asian monsoon. *Adv. Atmos. Sci.* **40**, 1429–1456 (2023).
45. Yu, T., Chen, W., Huang, P., Feng, J. & Jiang, N. Recent interdecadal changes in the tropospheric biennial oscillation of the East Asian summer monsoon. *Atmos. Res.* **277**, 106301 (2022).
46. Yu, T., Feng, J., Chen, W. & Chen, S. The interdecadal change of the relationship between North Indian Ocean SST and Tropical North Atlantic SST. *J. Geophys. Res. Atmos.* **127**, 1–14 (2022).
47. Zhang, W., Yu, Z., Jiang, F., Geng, X. & Zhang, R. Important role of the ENSO combination mode in the maintenance of the anomalous anticyclone over the western North Pacific in boreal summer. *Sci. China Earth Sci.* **65**, 1379–1387 (2022).
48. Zhu, Y., Wang, H., Zhou, W. & Ma, J. Recent changes in the summer precipitation pattern in East China and the background circulation. *Clim. Dyn.* **36**, 1463–1473 (2011).
49. Han, X. & Wang, C. Weakened feedback of the Indian Ocean on El Niño since the early 1990s. *Clim. Dyn*. https://doi.org/10.1007/s00382-021-05745-5 (2021).
50. He, Z. et al. Change in coherence of summer rainfall variability over the Western Pacific around the early 2000s: ENSO influence. *J. Clim.* **33**, 1105–1119 (2020).
51. Huang, Z., Zhang, W., Geng, X. & Jin, F. F. Recent shift in the state of the western Pacific subtropical high due to ENSO change. *J. Clim.* **33**, 229–241 (2020).
52. Li, X. & Lu, R. Breakdown of the summertime meridional teleconnection pattern over the western North Pacific and East Asia since the early 2000s. *J. Clim.* **33**, 8487–8505 (2020).
53. Sun, L., Yang, X., Tao, L., Fang, J. & Sun, X. Changing impact of ENSO events on the following summer rainfall in Eastern China since the 1950s. *J. Clim.* **34**, 8105–8123 (2021).
54. Wang, X., Hu, Z. Z., Hu, P., Ye, J. & Feng, G. The weakening relationship between ENSO and the following summer Pacific Japan teleconnection since the late 1990s. *Clim. Dyn.* **61**, 4033–4046 (2023).
55. Xu, P., Wang, L., Chen, W., Feng, J. & Liu, Y. Structural changes in the Pacific-Japan pattern in the late 1990s. *J. Clim.* **32**, 607–621 (2019).
56. Yang, X. & Huang, P. Restored relationship between ENSO and Indian summer monsoon rainfall around 1999/2000. *Innov* **2**, 100102 (2021).
57. Ding, Y. & Chan, J. C. L. The East Asian summer monsoon: an overview. *Meteorol. Atmos. Phys.* **89**, 117–142 (2005).
58. Yin, Z. et al. Traditional Meiyu–Baiu has been suspended by global warming. *Natl. Sci. Rev*. **11**, nwae166 (2024).
59. Wang, C., Zheng, X. & Song, F. Enhanced mid-to-late summer precipitation over midlatitude East Asia under global warming. *J. Clim.* **37**, 4221–4237 (2024).
60. Jiang, W. et al. Northwest Pacific anticyclonic anomalies during post-El Niño summers determined by the pace of El Niño decay. *J. Clim.* **32**, 3487–3503 (2019).
61. Kawamura, R., Matsuura, T. & Iizuka, S. Role of equatorially asymmetric sea surface temperature anomalies in the Indian Ocean in the Asian summer monsoon and El Niño-Southern oscillation coupling. *J. Geophys. Res. Atmos.* **106**, 4681–4693 (2001).
62. Wu, Z., Li, J., Jiang, Z., He, J. & Zhu, X. Possible effects of the North Atlantic oscillation on the strengthening relationship between the East Asian Summer monsoon and ENSO. *Int. J. Climatol.* **32**, 794–800 (2012).
63. Yang, S. et al. El Niño-Southern oscillation and its impact in the changing climate. *Natl. Sci. Rev.* **5**, 840–857 (2018).
64. Cai, W. et al. Pantropical climate interactions. *Science* **363**, 1–3 (2019).
65. Wang, C. Three-ocean interactions and climate variability: a review and perspective. *Clim. Dyn.* **53**, 5119–5136 (2019).
66. Ma, J., He, W., Chen, Z., Fu, Y. & Yin, J. The impact of north tropical Atlantic sea surface temperature anomalies in the ensuing spring of El Niño on the tropical Indian Ocean and Northwest Pacific. *Int. J. Climatol.* **40**, 4978–4991 (2020).
67. Ham, Y. G., Kug, J. S., Park, J. Y. & Jin, F. F. Sea surface temperature in the north tropical Atlantic as a trigger for El Niño/Southern oscillation events. *Nat. Geosci.* **6**, 112–116 (2013).
68. Yang, Y., Zhu, Z., Shen, X., Jiang, L. & Li, T. The influences of Atlantic sea surface temperature anomalies on the ENSO-independent interannual variability of East Asian summer monsoon rainfall. *J. Clim.* **36**, 677–692 (2023).
69. Takaya, Y., Saito, N., Ishikawa, I. & Maeda, S. Two tropical routes for the remote influence of the northern tropical Atlantic on the indo-western Pacific summer climate. *J. Clim.* **34**, 1619–1634 (2021).
70. Feng, J. & Chen, W. Respective and combined impacts of north Indian Ocean and tropical North Atlantic SST anomalies on the sub-seasonal evolution of anomalous western North Pacific anticyclone. *J. Clim*. 1–30 https://doi.org/10.1175/jcli-d-21-0799.1 (2022).
71. Wang, L., Yu, J. Y. & Paek, H. Enhanced biennial variability in the Pacific due to Atlantic capacitor effect. *Nat. Commun*. **8**, (2017).
72. McGregor, S. et al. Recent Walker circulation strengthening and Pacific cooling amplified by Atlantic warming. *Nat. Clim. Chang.* **4**, 888–892 (2014).
73. Hong, C. C., Chang, T. C. & Hsu, H. H. Enhanced relationship between the tropical Atlantic SST and the summertime western north pacific subtropical high after the early 1980s. *J. Geophys. Res.* **119**, 3715–3722 (2014).
74. Li, X., Xie, S. P., Gille, S. T. & Yoo, C. Atlantic-induced pan-tropical climate change over the past three decades. *Nat. Clim. Chang.* **6**, 275–279 (2016).
75. Fan, L. Understanding the interdecadal changes in the teleconnection pattern of the East Asian summer monsoon precipitation with concurrent ENSO. https://doi.org/10.1029/2024GL111723 (2024).
76. Takaya, Y., Ishikawa, I., Kobayashi, C., Endo, H. & Ose, T. Enhanced Meiyu-Baiu rainfall in early summer 2020: aftermath of the 2019 super IOD event. *Geophys. Res. Lett.* **47**, 1–9 (2020).
77. Wang, C. Y., Zheng, X. T. & Xie, S. P. Enhanced ENSO-unrelated summer variability in the Indo–Western Pacific under global warming. *J. Clim.* **36**, 1749–1765 (2023).
78. Chen, S. et al. Interdecadal variation in the impact of Arctic Sea Ice on the El Niño-Southern oscillation: the role of atmospheric mean flow. *J. Clim*. https://doi.org/10.1175/jcli-d-23-0733.1 (2024).
79. Kobayashi, S. et al. The JRA-55 reanalysis: general specifications and basic characteristics. *J. Meteorol. Soc. Japan* **93**, 5–48 (2015).
80. Harada, Y. et al. The JRA-55 reanalysis: representation of atmospheric circulation and climate variability. *J. Meteorol. Soc. Japan* **94**, 269–302 (2016).
81. Kanamitsu, M. et al. NCEP-DOE AMIP-II reanalysis (R-2). *Bull. Am. Meteorol. Soc*. **83**, (2002).
82. Hersbach, H. et al. The ERA5 global reanalysis. *Q. J. R. Meteorol. Soc.* **146**, 1999–2049 (2020).
83. Rayner, N. A. et al. Global analyses of sea surface temperature, sea ice, and night marine air temperature since the late nineteenth century. *J. Geophys. Res. Atmos*. **108**, (2003).
84. Huang, B. et al. Extended reconstructed sea surface temperature, version 5 (ERSSTv5): upgrades, validations, and intercomparisons. *J. Clim.* **30**, 8179–8205 (2017).
85. Kaplan, A. et al. Analyses of global sea surface temperature 1856-1991. *J. Geophys. Res. Ocean.* **103**, 18567–18589 (1998).
86. Xie, P. & Arkin, P. A. Global precipitation: a 17-year monthly analysis based on gauge observations, satellite estimates, and numerical model outputs. *Bull. Am. Meteorol. Soc.* **78**, 2539–2558 (1997).
87. Yu, L. & Weller, R. A. Objectively analyzed air-sea heat fluxes for the global ice-free oceans (1981-2005). *Bull. Am. Meteorol. Soc.* **88**, 527–539 (2007).
88. Wang, B. & Fan, Z. Choice of South Asian summer monsoon indices. *Bull. Am. Meteorol. Soc.* **80**, 629–638 (1999).
89. Wang, B. et al. How to measure the strength of the East Asian summer monsoon. *J. Clim.* **21**, 4449–4463 (2008).

90. Hoerling, M. P., Kumar, A. & Zhong, M. El Niño, La Niña, and the nonlinearity of their teleconnections. *J. Clim.* **10**, 1769–1786 (1997).
91. Tao, W. et al. Asymmetry in summertime atmospheric circulation anomalies over the northwest Pacific during decaying phase of El Niño and La Niña. *Clim. Dyn.* **49**, 2007–2023 (2017).
92. Wu, B., Li, T. & Zhou, T. Asymmetry of atmospheric circulation anomalies over the western north Pacific between El Niño and La Niña. *J. Clim.* **23**, 4807–4822 (2010).
93. Eyring, V. et al. Overview of the coupled model intercomparison project phase 6 (CMIP6) experimental design and organization. *Geosci. Model Dev.* **9**, 1937–1958 (2016).
94. Kosaka, Y. & Xie, S. P. The tropical Pacific as a key pacemaker of the variable rates of global warming. *Nat. Geosci.* **9**, 669–673 (2016).

Acknowledgements

We sincerely thank the editor and anonymous reviewers for their constructive suggestions, which helped to improve the paper. We acknowledge the World Climate Research Program's Working Group on Coupled Modeling and the Climate Variability and Change Working Group (CVCWG) for producing and making available their model output. This study was supported by the Yunnan International Joint Laboratory of Monsoon and Extreme Climate Disasters (Award number 202403AP140009) and the National Natural Science Foundation of China (Grants 42230605, 42475039 and 42425504).

Author contributions

T.Y., W.C., and P.H. conceived the study, performed the analyses, and wrote the paper. G.H. gave comments and contributed to improving the paper. X.Y. contributed to the model results.

Competing interests

The authors declare no competing interests.

Additional information

Supplementary information The online version contains supplementary material available at https://doi.org/10.1038/s41612-025-00983-4.

Correspondence and requests for materials should be addressed to Wen Chen or Ping Huang.